Talanta 283 (2025) 127150

Contents lists available at ScienceDirect

Talanta

journal homepage: www.elsevier.com/locate/talanta

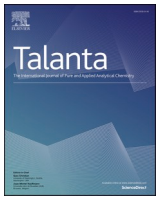

Preparation of gelatine calibration standards for LA-ICP-MS bioimaging with 266 nm laser ablation systems

Thomas E. Lockwood, Dayanne C.M. Bordin, Mika T. Westerhausen, David P. Bishop *

Hyphenated Mass Spectrometry Laboratory, University of Technology Sydney, Ultimo, NSW, Australia

ARTICLE INFO

Keywords:
Laser ablation
Gelatine
Calibration
Interferometry
Profilometry

ABSTRACT

Gelatine is the external standard matrix of choice for quantitative biomaging of elements and metal tags in tissue. Its ablation characteristics closely match that of tissue when using 193 and 213 nm lasers, but this has not been demonstrated at 266 nm. With the interest in 266 nm laser ablation systems growing due to the selective ablation of tissue over glass substrates, this gap needed to be investigated. Optical profilometry was used to map the line crater volumes of gelatine and murine brain and quadriceps tissues ablated with a 266 nm laser. Raw gelatine did not ablate in a similar manner to either tissue type and ultra-violet absorbent chemical additives were required to match ablation volumes. Addition of either 4 g L^{-1} L-tryptophan or 3 g L^{-1} gallic acid was used to match the ablation volume of murine quadriceps. Murine brain tissue had an increased ablation volume over the quadriceps tissue (1400 ± 130 versus 1100 ± 160 μm^3 at 1.5 J cm^{-2}), and the addition of 5 g L^{-1} gallic acid and the use of low laser energy (≤1.5 J cm^{-2}) was required to match the ablation of brain tissue. The modified standards were tested on a 213 nm laser, and the addition of either additive to gelatine did not affect ablation volume. The effect of additives on fractionation and two-phase sample transport was investigated, no fractionation was observed, and a decrease in two-phase sample transport of up to 60 % was obtained with the modified gelatine. This decrease was caused by the reduced laser energy required for ablation. Finally, the potential uses of optical profilometry as a standardisation tool are discussed.

1. Introduction

Laser ablation-inductively coupled plasma-mass spectrometry (LA-ICP-MS) is a powerful tool for the quantitative imaging of both endogenous and exogenous metals, and metal-tagged biomolecules in tissue sections. LA-ICP-MS has been applied to a range of biological samples and pathologies, achieving sub mg kg^{-1} limits of analysis and spatial resolutions down to a single μm [1]. Applications include the investigation of heavy metals in murine tissue [2] and rice [3], nanomaterials [4], and the role of metals in Alzheimer's [5] and breast cancer [6]. Like all quantitative techniques, LA-ICP-MS requires appropriate standards for external calibration, and much research has focused on material selection and fabrication methods for these standards [7].

Homogenised tissue, either in the form of a certified reference material (CRM) [8] or prepared in-house [9], is a common calibration approach for the imaging of soft tissue. However, due to the limited availability of suitable CRMs, difficulties in preparation of homogenised tissue, and relatively poor analytical figures of merit, gelatine has rapidly become the standard surrogate matrix used to prepare external calibration standards for quantitative bioimaging of tissues. Compared to the use of homogenised tissue, gelatine is easier to handle, more homogenous, and contains lower concentrations of endogenous elements [10]. Gelatine standards can also be prepared using a variety of methods, including sectioning [11], moulding [10], and spotting [12,13] to achieve a desired form and thickness. Other materials such as PMMA and egg yolk have also been proposed but are more difficult to handle and more removed in composition from soft tissue [14,15]. A comprehensive review of calibration approaches for bioimaging by LA-ICP-MS is available from Mervič et al. [7].

Tissue strongly absorbs deep ultra-violet (UV) light around 190 nm, due to the abundance of peptide bonds, making 193 nm lasers highly effective for tissue ablation [16]. However, 193 nm lasers are also absorbed well by glass, potentially leading to co-ablation of the glass slides used to mount samples [17]. In contrast, 266 nm lasers (the Nd:YAG fourth harmonic) have the ability to ablate tissue samples without simultaneously ablating the glass substrates they are mounted on. The ablation threshold of glass is higher at 266 nm than 193 nm due to lower coupling, and manufacturers are now developing 266 nm systems

* Corresponding author. PO Box 123, Ultimo, NSW, 2007, Australia.
E-mail address: david.bishop@uts.edu.au (D.P. Bishop).

https://doi.org/10.1016/j.talanta.2024.127150
Received 11 July 2024; Received in revised form 17 October 2024; Accepted 2 November 2024
Available online 2 November 2024

specifically for bioimaging [18] that have featured in the literature [19–21]. However, these systems are less common compared to 193 nm and 213 nm lasers, and the standard calibration strategies employed for these wavelengths have yet to be tested.

Gelatine has been shown to have very similar ablation properties to tissue samples with a 193 nm laser [10]. However, the presence of DNA and aromatic amino acids in tissue creates additional absorbances in the 240–290 nm region [22]. Gelatine is derived from collagen, a protein that is almost devoid of aromatic amino acids, and only weakly absorbs in this region [16,22]. This, coupled with the absence of other biological components, create a material that has notably different ablation properties to tissue at a wavelength of 266 nm.

A recent publication by Van Helden et al. has also shown that the sample transport for biological material is wavelength dependant, with increased two-phase (particulate and gas) formation at higher wavelengths. This formation was exaggerated at higher wavelengths (213 nm) and can lead to blurring, potentially requiring a reduction in data acquisition rates [16] and decreasing the utility of current generation high-speed laser ablation systems [23].

The gelatine matrix in its native form is a mismatched-matrix to tissue when using a 266 nm laser. Additives are frequently used to target or improve ablation of materials by increasing absorbance at a target wavelength [24]. Here, we used widely available compounds to increase the absorbance of gelatine at 266 nm and compare the ablation of tissue and gelatine at 213 and 266 nm. A range of compounds and concentrations were tested to match the ablated volume of gelatine and tissue, as measured using optical profilometry and atomic force microscopy (AFM), with the optimal additives and concentrations for quantitative LA-ICP-MS bioimaging with a 266 nm laser described.

2. Materials and methods

2.1. Preparation of standards

Food-grade azo dyes were supplied by All Colour Supplies (Padstow, Australia). Acridine orange, gallic acid (3,4,5-Trihydroxybenzoic acid) and L-tryptophan were purchased from Sigma Aldrich (Castle Hill, Australia). Gelatine standards were prepared as per Westerhausen et al. with addition of UV absorbents to the buffer [10]. Briefly, 100 mg of porcine gelatine (Sigma Aldrich) was spiked with individual dissolved metal standards (10 or 1000 ppm in 2 % HNO_3; High Purity Standards; Choice Analytical; Thornleigh, Australia) and made up to 1 ml with a 100 mM Tris-HCl, 10 mM EDTA buffer. The 10 % gelatine solution was heated at 45 °C on a heat block until completely dissolved. Solutions were then pipetted into Grace Bio-Labs HybriWell™ sealing systems (Sigma Aldrich) adhered to glass microscope slides. Slides were frozen at −80 °C for 5 min, the HybriWell™ seals removed, and gelatine dried in a desiccator overnight. UV absorbent additives were added to the buffer at five concentrations between 1 and 5 g L^{-1} prior to addition of the buffer to the gelatine, corresponding to 1–5 % dry weight.

2.2. Tissue samples

Murine brains were harvested at the Florey Institute of Neuroscience and Mental Health (Melbourne, Australia) under Animal Care and Ethics protocol 15-104-FINMH. Briefly, animals were euthanised with an overdose of sodium pentobarbitone and perfused with warmed phosphate buffered saline. Frozen brains were cryo-sectioned at a thickness of 30 μm on a CryoStar® cryotome (Thermo Fisher; North Ryde, Australia) using a PTFE-coated blade (DT315R50; C. L. Sturkey, Inc.; Lebanon, PA) and mounted onto glass slides.

Murine quadriceps tissues were harvested from mice maintained following guidelines established by the Institutional Animal Care and Use Committee at the University of California, Los Angeles, and approval for the mice in this study was granted by the UCLA Institutional Animals Care and Use Committee (#2000-029-61D). Muscles were frozen in OCT, sectioned and stored at −80 °C until use.

2.3. LA-ICP-MS

Laser ablation experiments were performed on an ESL imageBIO266 (Kenelec Scientific, Mitcham, Australia) equipped with a TwoVol3 ablation chamber and coupled to an Agilent 7900 series ICP-MS (Mulgrave, Australia) operated using the parameters in Table S1. Line based experiments used a 20 μm spot size, scan speed of 800 μm s^{-1}, 200 Hz firing rate and 16 μm spot overlap, resulting in five ablations per spot width. A transfer line length of 40 cm was used.

Confirmation of ablation volume and signal intensity was performed by ablating the L-tryptophan (0–5 g L^{-1}) containing gelatine, spiked to a final approximate concentration of 40 μg kg^{-1} (dry weight) with Sc, Y, Pr and Ho from High Purity Standards. A laser fluence of 1.5 J cm^{-2} and the parameters specified above were used.

Single-pulse response profiles were performed using 20 μm spots with a firing rate of 1000 Hz and dosage of 5 at 1 s intervals. The laser ablation system was coupled to the ICP-MS using a 2.5 m transfer tube to enhance the separation of the phases. Data was collected for 50 spots per element (approximately 40 μg kg^{-1} (dry weight) As, Cd, Cu, Zn) with an acquisition time of 0.001 s.

Quantification of the murine brain was performed at a 20 μm spot size, speed of 400 μm s^{-1}, 200 Hz laser repletion rate, 18 μm overlap [23] and fluence of 1.5 J cm^{-2}. Six standard levels containing 5 g L^{-1} gallic acid and up to 10 mg kg^{-1} Mn and Cu and 500 mg kg^{-1} Fe and Zn were prepared using chelated porcine gelatine, as per the procedure in Westerhausen et al. [10]. Briefly, 2 g chelator (Amberlite IR120-Na+ (Sigma Aldrich)) per 1 g gelatine was added to a 20 % gelatine solution, agitated at 40 °C for 1 h and centrifuged to remove the chelator. The standards were then prepared using the same procedure as above with aliquots taken for digestion and concentrations determined using solution nebulisation ICP-MS.

Data was processed in Python 3.12 using the NumPy and SciPy libraries.

2.4. Analysis of ablation volume

Optical profilometric measurements of samples and standards were performed using a Filmetrics Profilm3D (Warsash Scientific; Redfern, Australia). Topography measurements were made using green-light interferometry through a 20X objective, correlating to a pixel resolution of 0.871 μm and a total imaged area of 564 × 422 μm. Three consecutive measurements were averaged and remaining invalid pixels in the profile data interpolated using Clough-Tocher cubic interpolation.

To determine significance of differences in ablation volume, asymptotic two-sided Mann-Whitney U tests with tie correction were used. Each sample consisted of the total ablation volume from 128 'pixels' (20 × 20 μm ablations). This test was chosen due to its non-parametric nature and the unknown nature of the underlying ablation volume distributions.

Atomic force microscopy (AFM) was performed using a Park XE7 AFM (scitek, Lane Cove, Australia) operating in non-contact mode using a HQ:NSC15/Al tip (MikroMasch, Sofia, Bulgaria) and an XYZ resolution of 0.25 x 0.25 × 0.0001 μm. 5 μm lines were created using laser ablation at an energy density of 1.5 J cm^{-2} and dosage of 5 and then topography was mapped using AFM.

3. Results and discussion

Gallic acid and L-tryptophan (the amino acid responsible for 240–280 nm absorbance in proteins) were chosen as the ablation enhancing additives due to their strong absorbance at 266 nm. A range of azo-based food grade dyes were also tested due to their availability and compatibility with gelatine but were eliminated due to poor absorbance (Table S2). Acridine dyes have excellent absorbance at 266

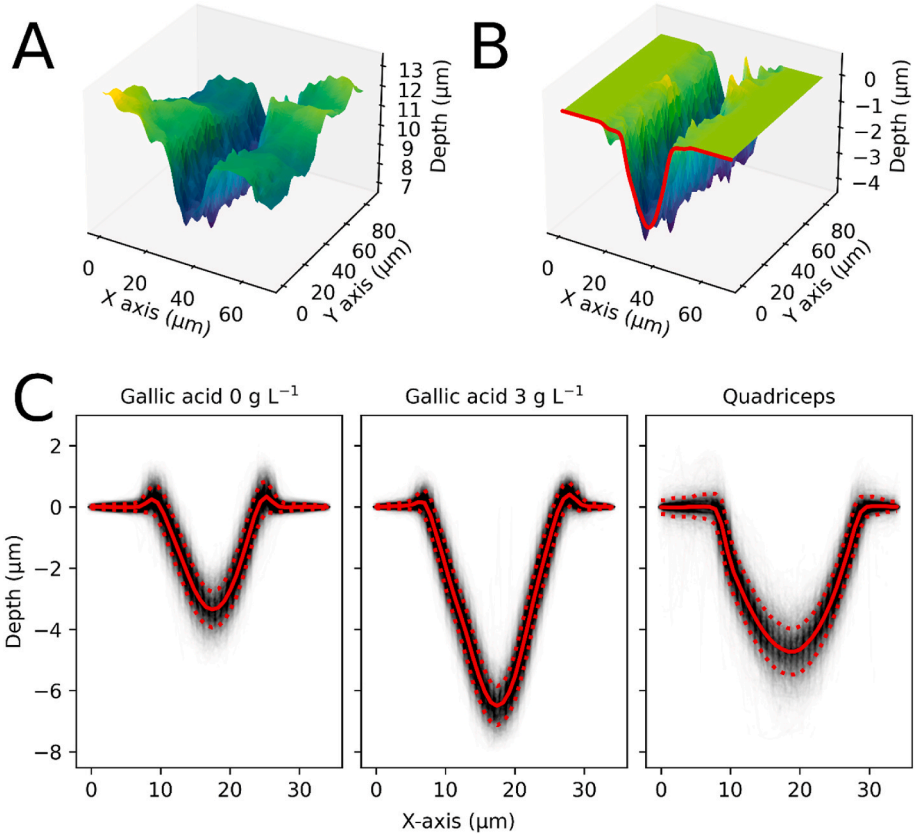

Fig. 1. (A) Profile of the ablation trench in murine quadriceps. (B) The trench in (A) post alignment and interpolation, the mean profile is shown in red. (C) Extracted profiles. Means and standard deviations are shown in solid and dotted red lines.

nm and addition of acridine orange to gelatine was able to match the ablation characteristics of murine brain at a relatively low concentration (2 g L^{-1}, see Fig. S1). However, its use was discontinued due to persistent zinc contamination, preventing the quantification of an important biological element.

Gallic acid can complex with metal ions, such as Fe^{2+} and Zn^{3+}, which results in a shift in peak absorbance from around 260 to 290 nm [25]. Preliminary experiments indicated that a gallic acid concentration greater than 1 g L^{-1} was required, and it would therefore be in excess to the total concentration of metals generally added to external calibration standards. To ensure this did not interfere with ablation, a standard was prepared with 5 g L^{-1} gallic acid and 250 mg kg^{-1} (dry weight) Fe and Zn. The standard was ablated, and the resulting ablation volumes (510 ± 80 versus 520 ± 50 μm^3) were not greater than gelatine without added metals (Mann-Whitney U; $p = 0.94$).

Fresh-frozen murine muscle and brain tissue were chosen as representative samples due to their extensive use in our laboratory, but other tissue types and preparation methods may have different ablation characteristics. In particular, tissue fixing methods such as formalin-fixed paraffin-embedded can increase the ablation threshold [13].

3.1. Matching gelatine and tissue ablation volume

To determine the concentration of gallic acid or L-tryptophan required to match the ablation characteristics of gelatine to tissue, a series of standards were prepared at a range of concentrations (0–5 g L^{-1}). Lines were then ablated in the standards and tissues using laser fluences of 1.0, 1.5 and 2.0 J cm^{-2}. These fluences represent the range of 'tissue friendly' energy densities (on our system), where the tissue was ablated but the glass was not. This is typically below 0.5 J cm^{-2} for a 193 nm laser, but was higher at 266 nm due to lower excitation efficiency [17,18]. Low energies are also important for preserving nanoparticles embedded in tissue [26]. As gelatine is used as a standard matrix for tissue, we focused on matching ablation crater volume (i.e., the amount of material removed for a given ablation event) rather than the topography of ablated craters. This ensured that the same concentration gelatine and tissue material produced the same ICP-MS signal, the foremost requirement of a standard matrix. Measured ablation volumes correlated to the signals recorded on the ICP-MS across the mass range ($r^2 > 0.985$; Fig. S2).

The volume of material ablated was determined from the topography of the ablated craters, measured using optical profilometry. An area encompassing a total of 128 ablation regions (20 × 20 μm) was processed for each standard and tissue sample. Data was re-aligned to remove any vertical offsets from imperfect alignment of the sample to the profilometer stage during measurement, and linear interpolation of the unablated regions between lines were used to flatten data (Fig. 1A and B). The line-segment volumes were then calculated by integrating the resulting curves. Measurement variation was highest for the tissue samples due to their high surface roughness, with an average roughness (Sa) of 0.98 and 0.67 μm for muscle and brain, versus 0.20 μm for gelatine. Ablation of gelatine created a rim around the craters edge, indicative of thermalisation, that had to be accounted for to accurately assess the volume of ablation [27].

Unmodified gelatine did not ablate at 1.0 J cm^{-2} confirming the need for better correlation of ablation characteristics, and laser fluences greater than 2.0 J cm^{-2} resulted in complete ablation of even 50 μm sectioned samples, preventing the measurement of craters. The average volume of tissue ablated at 1.0, 1.5 and 2.0 J cm^{-2} was 700 ± 300, 1100 ± 160 and 1660 ± 180 μm^3 for murine quadriceps, and 810 ± 180, 1400 ± 130 and 2060 ± 180 μm^3 for murine brain. Lipids make up more than 50 % of the brain's dry weight [28], and have different ablation characteristics than low-fat tissues like muscle, accounting for the increased volume [29].

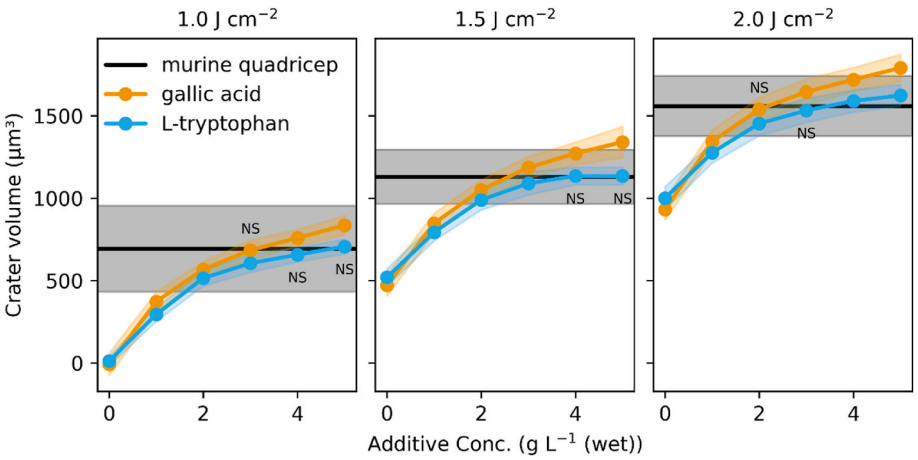

Fig. 2. Ablation volumes of gallic acid and L-tryptophan spiked gelatine compared with that of murine quadriceps. NS = no significant difference (Mann-Whitney U, $p > 0.05$). Standard deviation is indicated by the shaded areas.

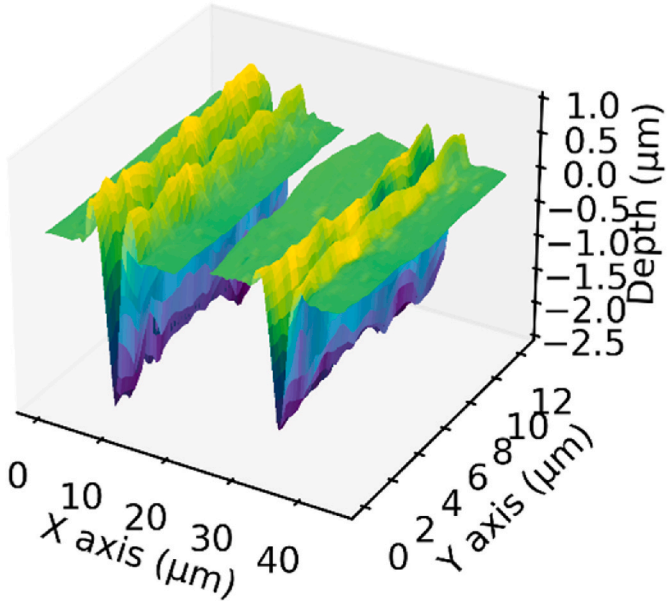

Fig. 3. Atomic force microscopy images of ablation craters in L-tryptophan spiked gelatine (left) and murine quadriceps.

The concentrations of additives required to match muscle tissue ablation volumes are shown in Fig. 2 and Table S2. A concentration of 3 g L^{-1} gallic acid or 4 g L^{-1} L-tryptophan matched well across all energy densities. The difference in volume was measured as 1, 5, and 6 % for gallic acid at 1.0, 1.5, and 2.0 J cm^{-2} respectively, and 5, 0.4, and 2 % for L-tryptophan. There was no significant difference in the ablation volume at 1.0 J cm^{-2} for 3 g L^{-1} gallic acid (Mann-Whitney U, $p = 0.89$) nor at 1.0 and 1.5 J cm^{-2} for 4 g L^{-1} L-tryptophan (Mann-Whitney U; $p = 0.34$, 0.87). The addition of either gallic acid or L-tryptophan can therefore lower the ablation threshold of gelatine to match the ablated volume of muscle tissue. While the variance in ablation volume did increase at higher additive concentrations, the relative standard deviation remained constant (4–6 %).

To test if ablation volume matching was consistent at different laser spot sizes, a sample of mouse quadriceps and the 4 g L^{-1} L-tryptophan spiked gelatine was ablated using a 5 µm spot size at 1.5 J cm^{-2} and a dosage of 5. The resulting craters, plotted in Fig. 3, were then measured using AFM, due to the insufficient resolution of the optical profilometer. Again, the ablated crater volumes were not significantly different (Mann-Whitney U; $p = 0.62$).

The required concentration of additives to match the ablation of brain tissue was found to be fluence dependent, and fluences of 2.0 J cm^{-2} and above were unable to be matched (Fig. S3). This is hypothesised to be caused by the tissue's high fat content increasing its rate of ablation [29]. L-tryptophan was insufficient at all laser energies, even at the highest concentration of 5 g L^{-1}. Therefore, gallic acid is the more suitable additive when analysing brain tissue. A concentration of 5 g L^{-1} gallic acid reduced the difference in ablated volume from 100 to 3 % and from 66 to 4 % for 1.0 and 1.5 J cm^{-2}. There was no significant difference in ablated volume between 5 g L^{-1} gallic acid and brain tissue at 1.0 J cm^{-2} (Mann-Whitney U; $p = 0.08$). Even though the ablated volume could not be matched at an energy density of 2.0 J cm^{-2}, the difference in volume was reduced from 55 to 13 % by addition of gallic acid. While higher concentrations of gallic acid could be made, the impact on ablation only grows logarithmically and its solubility is low (11.9 g L^{-1} in water).

3.2. Ablation performance of optimised gelatine at 213 nm

The optimised gelatine standards were ablated using a 213 nm laser to assess their compatibility across different wavelengths. Gelatine with and without 4 g L^{-1} of L-tryptophan was ablated at an energy density of 2.96 J cm^{-2}. There was no significant difference in the volume of ablated material, confirming that the increase in ablation is from increased absorption at 266 nm (Mann-Whitney U; $p = 0.14$).

The crater volume of murine quadriceps and brain tissue was similar (Mann-Whitney U; $p = 0.18$), indicating that the increased ablation of brain seen at 266 nm is a result of the higher wavelength. Increased ablation of fatty tissue has also been observed during ablation using a 355 nm laser [29]. Extracted profiles for the gelatine and tissue samples are shown in Fig. S4.

3.3. Fractionation and sample transport of optimised gelatine

Fractionation has been observed in gelatine standards when laser powers near the threshold of ablation are used. This is hypothesised to be caused by preferential release of less strongly bound species into the gas phase [30]. To determine the effects of the additives on fractionation a 4 g L^{-1} L-tryptophan spiked standard containing equal concentrations of U and Th was prepared and ablated at laser fluences from 1 to 2 J cm^{-2}. As shown in Fig. S5, fractionation (reported as the $^{238}U/^{232}Th$ ratio [31]) was reduced for each laser fluence in the modified gelatine. At 1.0 J cm^{-2} a ratio of 1.14 ± 0.18 was observed, indicating fractionation as reported in the literature. At fluences of 1.25 J cm^{-2} and above

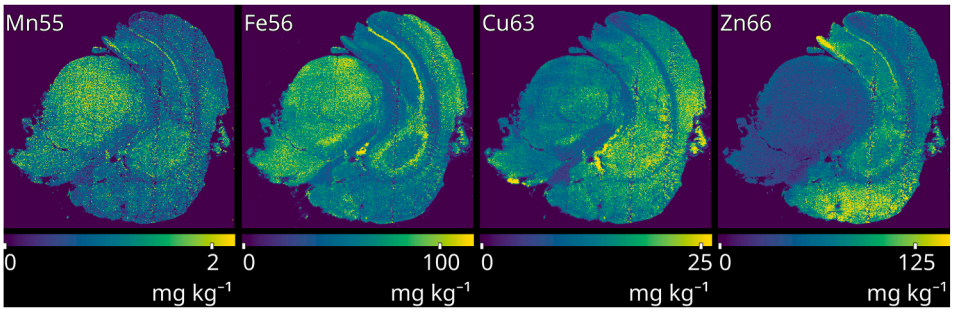

Fig. 4. Quantities of Mn, Fe, Cu and Zn in murine brain using the 5 g L^{-1} gallic acid modified gelatine standards. Spikes have been removed using a windowed median filter.

the fractionation decreased and stabilised at 1.03 ± 0.10. These results echo those reported in the literature and suggest that fractionation is only an issue for gelatine standards at powers near the ablation threshold [30].

The formation of a gas phase, in addition to a particle phase, during ablation was recently shown to be more prevalent with higher wavelength lasers. The gas phase was transported slower than the particulate phase, which led to a lengthened washout time and smearing of images [16].

To test the effects of the gallic acid on reducing two-phase sample transport, both the modified and unmodified gelatine was ablated to measure the single pulse response profiles. The signal produced by a single ablation event was matched by raising the energy density used to ablate the un-modified gelatine, with 2.5 J cm^{-2} required to match that produced at 1 J cm^{-2} for the modified gelatine. Elements previously identified to have increased gas phase formation at higher wavelengths (As, Cd, Cu, Zn) were monitored and profiles were obtained for both gelatine standards (Fig. S6) [16]. Reduced gas phase formation was observed for As, Cd and Zn (46, 60 and 45 % reduce in peak height) when ablating the gallic acid spiked gelatine, due to the lower energy density. This was confirmed by ablating both the standards at the higher laser energy (2.5 J cm^{-2}), which produced the identical profiles in Fig. S7. Two-phase formation was not observed for Cu in any experiment. This energy is more than double that required to ablate tissue and the modified gelatine.

A larger gas phase was observed than in previous studies on 193 and 213 nm lasers, suggesting that two-phase sample transport is increased during ablation at 266 nm. However, the experiments in the referenced and present study were performed with a very long (2.5 m) transfer line and, under standard operating conditions with a 40 cm transfer line, the impact of two-phase transport was negligible, with average transport of 5 ms (Fig. S8).

3.4. The importance of ablation volume

Despite a large amount of research into the creation and performance of gelatine calibration standards, important metrics like the volume of ablation is rarely measured and compared to those of tissue samples. While gelatine has been shown to have similar ablation characteristics to tissue on 193 nm lasers, this work has not been performed for 213 or 266 nm [17], and in this study we observed differing ablation crater shapes across materials for both 213 and 266 nm lasers. Current users of 266 nm rely on complete sample ablation and uniformly thick gelatine and tissue samples to avoid these issues [20,21]. However, the shrinkage of tissue during drying is variable, even within a single tissue sample, and is not comparable with gelatine, which shrinks to its dry mass (i.e. 10 % of its original thickness for a 10 % solution). We have previously shown that the thickness of cryo-sectioned gelatine and tissue is highly variable [10] and this was also observed in the current study. Brain cut at 20 and 30 μm had final average thicknesses of 8.3 and 12 μm for white matter, and 9.4 and 15 μm for grey matter, 41 and 48 % of the nominal thickness. Quadricep cut at 30 and 50 μm had final average thicknesses of 3.8 and 7.0 μm, only 13 % of the nominal thickness. Standard deviation of thickness across the tissue sections was as high as 24 % (30 μm quadriceps).

Despite these issues the cryo-sectioning of gelatine at the same thickness as tissue samples remains common [32,33], although some studies acknowledged this as a weakness, and attempt to match sample and standard shrinkage [21]. Future studies on calibration strategies for LA-ICP-MS should employ profilometry or other techniques to map sample and standard topography pre- and post-ablation. Other methods using non-matrix matched materials combined with optical profilometry to measure ablation volume have been proposed, but are time consuming when considering imaging large, heterogeneous samples [34].

3.5. Calibration of murine brain tissue

The analytical figures of merit of the calibration standards were characterised by quantifying Mn, Fe, Cu and Zn in a murine brain sample, see Fig. 4. Standards were prepared with endogenous levels of elements and 5 g L^{-1} gallic acid was used as a modifier, as brain is a high-lipid tissue. To accurately determine the metal contents the standards were cross-quantified using solution-nebulised ICP-MS. The linearity for all elements was acceptable (>0.98) and the addition of gallic acid did not raise the metal content of the chelated gelatine (Mn 7.9 versus 160 μg kg^{-1} for unchelated gelatine). Comprehensive figures of merit are available in Table S3.

4. Conclusion

Raw gelatine had a significantly higher ablation threshold at a wavelength of 266 nm than both murine quadriceps and brain tissue, and is an unsuitable matrix for calibration standards. The addition of either 3 g L^{-1} gallic acid or 4 g L^{-1} L-tryptophan lowered the ablation threshold to match that of murine quadriceps, and should be suitable for other low-fat tissues. Tissues with higher fat content, such as brain, have increased volumes of ablation at 266 nm and required a higher concentration of absorbing additives, with 5 g L^{-1} gallic acid being optimal at low energy densities. The lowered energy density required to ablate the modified gelatine decreased two-phase sample transport for elements of concern, which was furthermore mitigated by employing the shorter transfer lines typically used. While careful consideration of calibration strategies is required when using a 266 nm laser, the methods presented here allow calibration of both low and high fat tissues and could be replicated for tissues with intermediate fat content.

Funding sources

DBP is supported by an Australian Research Council Discovery Project (DP230101740).

CRediT authorship contribution statement

Thomas E. Lockwood: Writing – review & editing, Writing – original draft, Investigation, Formal analysis, Conceptualization. **Dayanne C.M. Bordin:** Writing – review & editing, Methodology, Investigation. **Mika T. Westerhausen:** Writing – review & editing, Investigation. **David P. Bishop:** Writing – review & editing, Resources, Conceptualization.

Declaration of competing interest

The authors declare that they have no known competing financial interests or personal relationships that could have appeared to influence the work reported in this paper.

Acknowledgements

The authors thank Associate Professor Hare for providing the murine brain, and Associate Professor Wanagat the murine quadriceps.

Appendix A. Supplementary data

Supplementary data to this article can be found online at https://doi.org/10.1016/j.talanta.2024.127150.

Data availability

Data will be made available on request.

References

[1] P.A. Doble, R.G. De Vega, D.P. Bishop, D.J. Hare, D. Clases, Laser ablation–inductively coupled plasma–mass spectrometry imaging in biology, Chem Rev 121 (2021) 11769–11822, https://doi.org/10.1021/acs.chemrev.0c01219.

[2] J. Liu, J. Cui, X. Wei, W. Li, C. Liu, X. Li, M. Chen, Y. Fan, J. Wang, Investigation on selenium and mercury interactions and the distribution patterns in mice organs with LA-ICP-MS imaging, Anal. Chim. Acta 1182 (2021) 338941, https://doi.org/10.1016/j.aca.2021.338941.

[3] T.E. Lockwood, R.B. Banati, C. Nikagolla, J.P. Violi, D.P. Bishop, Concentration and distribution of toxic and essential elements in traditional rice varieties of Sri Lanka grown on an Anuradhapura district farm, Biol. Trace Elem. Res. 202 (2024) 2891–2899.

[4] G. Marolt, S. Novak, A.J. Kokalj, I. Talaber, V. Kononenko, S. Loureiro, Z. Khodaparast, P.V. Silva, M.B. Fité, R.D. Handy, D. Drobne, High throughput laser ablation ICP-MS bioimaging of silver distribution in animal organisms and plant tissue after exposure to silver sulfide nanoparticles, J Anal At Spectrom 10 (2023), https://doi.org/10.1039/D3JA00223C, 1039.D3JA00223C.

[5] S. Junceda, M. Cruz-Alonso, B. Fernandez, R. Pereiro, E. Martínez-Pinilla, A. Navarro, Iron dysregulation in Alzheimer's disease: LA-ICP-MS bioimaging of the distribution of iron and ferroportin in the CA1 region of the human Hippocampus, Biomolecules 14 (2024) 295, https://doi.org/10.3390/biom14030295.

[6] R. Pamphlett, L. Satgunaseelan, S. Kum Jew, P.A. Doble, D.P. Bishop, Elemental bioimaging shows mercury and other toxic metals in normal breast tissue and in breast cancers, PLoS One 15 (2020) e0228226, https://doi.org/10.1371/journal.pone.0228226.

[7] K. Mervič, M. Šala, S. Theiner, Calibration approaches in laser ablation inductively coupled plasma mass spectrometry for bioimaging applications, TrAC Trends Anal Chem 172 (2024) 117574, https://doi.org/10.1016/j.trac.2024.117574.

[8] B. Jackson, S. Harper, L. Smith, J. Flinn, Elemental mapping and quantitative analysis of Cu, Zn, and Fe in rat brain sections by laser ablation ICP-MS, Anal. Bioanal. Chem. 384 (2006) 951–957, https://doi.org/10.1007/s00216-005-0264-6.

[9] D.J. Hare, J. Lear, D. Bishop, A. Beavis, P.A. Doble, Protocol for production of matrix-matched brain tissue standards for imaging by laser ablation-inductively coupled plasma-mass spectrometry, Anal. Methods 5 (2013) 1915, https://doi.org/10.1039/c3ay26248k.

[10] M.T. Westerhausen, T.E. Lockwood, R.G. de Vega, A. Röhnelt, D.P. Bishop, N. Cole, P.A. Doble, D. Clases, Low background mould-prepared gelatine standards for reproducible quantification in elemental bio-imaging, Analyst 144 (2019) 6881–6888, https://doi.org/10.1039/C9AN01580A.

[11] O. Hachmöller, M. Aichler, K. Schwamborn, L. Lutz, M. Werner, M. Sperling, A. Walch, U. Karst, Element bioimaging of liver needle biopsy specimens from patients with Wilson's disease by laser ablation-inductively coupled plasma-mass spectrometry, J. Trace Elem. Med. Biol. 35 (2016) 97–102, https://doi.org/10.1016/j.jtemb.2016.02.001.

[12] M. Šala, V.S. Šelih, J.T. Van Elteren, Gelatin gels as multi-element calibration standards in LA-ICP-MS bioimaging: fabrication of homogeneous standards and microhomogeneity testing, The Analyst 142 (2017) 3356–3359, https://doi.org/10.1039/C7AN01361B.

[13] A. Schweikert, S. Theiner, D. Wernitznig, A. Schoeberl, M. Schaier, S. Neumayer, B. K. Keppler, G. Koellensperger, Micro-droplet-based calibration for quantitative elemental bioimaging by LA-ICPMS, Anal. Bioanal. Chem. 414 (2022) 485–495, https://doi.org/10.1007/s00216-021-03357-w.

[14] O. Reifschneider, K.S. Wentker, K. Strobel, R. Schmidt, M. Masthoff, M. Sperling, C. Faber, U. Karst, Elemental bioimaging of thulium in mouse tissues by laser ablation-ICPMS as a complementary method to heteronuclear proton magnetic resonance imaging for cell tracking experiments, Anal. Chem. 87 (2015) 4225–4230, https://doi.org/10.1021/ac504363q.

[15] C. Austin, D. Hare, T. Rawling, A.M. McDonagh, P. Doble, Quantification method for elemental bio-imaging by LA-ICP-MS using metal spiked PMMA films, J Anal At Spectrom 25 (2010) 722, https://doi.org/10.1039/b911316a.

[16] T. Van Helden, K. Mervič, I. Nemet, J.T. Van Elteren, F. Vanhaecke, S. Rončević, M. Šala, T. Van Acker, Evaluation of two-phase sample transport upon ablation of gelatin as a proxy for soft biological matrices using nanosecond laser ablation – inductively coupled plasma – mass spectrometry, Anal. Chim. Acta 1287 (2024) 342089, https://doi.org/10.1016/j.aca.2023.342089.

[17] T. Van Acker, S.J.M. Van Malderen, L. Colina-Vegas, R.K. Ramachandran, F. Vanhaecke, Selective ablation of biological tissue and single cells on a glass substrate by controlling the laser energy density of nanosecond 193 nm laser radiation, J Anal At Spectrom 34 (2019) 1957–1964, https://doi.org/10.1039/C9JA00126C.

[18] I. Horn, D. Günther, The influence of ablation carrier gasses Ar, He and Ne on the particle size distribution and transport efficiencies of laser ablation-induced aerosols: implications for LA–ICP–MS, Appl. Surf. Sci. 207 (2003) 144–157, https://doi.org/10.1016/S0169-4332(02)01324-7.

[19] I. Abdelhalim, O. Hamdy, M.A. Khattab, S. Abdelkawi, S. Hassab Elnaby, A. A. Hassan, Evaluating the efficacy of Nd:YAG fourth harmonic (266 nm) in comparison with ArF excimer (193 nm) in laser corneal reshaping: ex vivo pilot study, Int. Ophthalmol. 43 (2023) 3087–3096, https://doi.org/10.1007/s10792-023-02708-z.

[20] P. Yamkate, S. Funke, K. Steiger, R.M. Gold, J.A. Lidbury, U. Karst, J.M. Steiner, Quantitative bioimaging of copper in frozen liver specimens from cats using laser ablation-inductively coupled plasma-mass spectrometry, J. Feline Med. Surg. 25 (2023), https://doi.org/10.1177/1098612X231186919, 1098612X231186919.

[21] S. Strekopytov, K. Billimoria, H. Goenaga-Infante, A systematic study of high resolution multielemental quantitative bioimaging of animal tissue using LA-ICP-TOFMS, J Anal At Spectrom 38 (2023) 704–715, https://doi.org/10.1039/D2JA00402J.

[22] A. Vogel, V. Venugopalan, Mechanisms of pulsed laser ablation of biological tissues, Chem Rev 103 (2003) 577–644, https://doi.org/10.1021/cr010379n.

[23] T.E. Lockwood, M.T. Westerhausen, D.P. Bishop, Multiplexed elemental bioimaging with quadrupole ICP-MS and high-frequency laser ablation systems, J Anal At Spectrom 39 (2024) 1125–1130.

[24] K.M. McNally, B.R.D. Gillings, J.M. Dawes, Dye-assisted diode laser ablation of carious enamel and dentine, Aust. Dent. J. 44 (1999) 169–175, https://doi.org/10.1111/j.1834-7819.1999.tb00218.x.

[25] S.M. El-Megharbel, R.Z. Hamza, Synthesis, spectroscopic characterizations, conductometric titration and investigation of potent antioxidant activities of gallic acid complexes with Ca (II), Cu (II), Zn(III), Cr(III) and Se (IV) metal ions, J. Mol. Liq. 358 (2022) 119196, https://doi.org/10.1016/j.molliq.2022.119196.

[26] D. Metarapi, M. Šala, K. Vogel-Mikuš, V.S. Šelih, J.T. Van Elteren, Nanoparticle analysis in biomaterials using laser Ablation−Single Particle−Inductively coupled plasma mass spectrometry, Anal. Chem. 91 (2019) 6200–6205, https://doi.org/10.1021/acs.analchem.9b00853.

[27] J. Gonzalez, C. Liu, S. Wen, X. Mao, R. Russo, Metal particles produced by laser ablation for ICP–MS measurements, Talanta 73 (2007) 567–576, https://doi.org/10.1016/j.talanta.2007.04.029.

[28] I. Carrié, M. Clément, D. De Javel, H. Francès, J.-M. Bourre, Specific phospholipid fatty acid composition of brain regions in mice: effects of n–3 polyunsaturated fatty acid deficiency and phospholipid supplementation, J. Lipid Res. 41 (2000) 465–472, https://doi.org/10.1016/S0022-2275(20)34485-0.

[29] K. Sun, H. He, X. Xia, H. Wu, L. Tao, X. Ma, Ablation of porcine subcutaneous fat and porcine aorta tissues by a burst-mode nanosecond-pulsed laser at 355 nm, J Biophotonics 16 (2023) e202200190, https://doi.org/10.1002/jbio.202200190.

[30] R. Niehaus, M. Sperling, U. Karst, Study on aerosol characteristics and fractionation effects of organic standard materials for bioimaging by means of LA-ICP-MS, J Anal At Spectrom 30 (2015) 2056–2065, https://doi.org/10.1039/C5JA00221D.

[31] T. Van Acker, S.J.M. Van Malderen, T. Van Helden, C. Stremtan, M. Šala, J.T. Van Elteren, F. Vanhaecke, Analytical figures of merit of a low-dispersion aerosol transport system for high-throughput LA-ICP-MS analysis, J Anal At Spectrom 36 (2021) 1201–1209, https://doi.org/10.1039/D1JA00110H.

[32] R. Buchholz, S. Krossa, M.K. Andersen, M. Holtkamp, M. Sperling, U. Karst, M.-B. Tessem, A simple preparation protocol for shipping and storage of tissue sections

for laser ablation-inductively coupled plasma-mass spectrometry imaging, Metallomics 14 (2022) mfac013, https://doi.org/10.1093/mtomcs/mfac013.
[33] J. Liu, L. Zheng, X. Wei, B. Wang, H. Chen, M. Chen, M. Wang, W. Feng, J. Wang, Quantitative imaging of trace elements in brain sections of Alzheimer's disease mice with laser ablation inductively coupled plasma-mass spectrometry, Microchem. J. 172 (2022) 106912, https://doi.org/10.1016/j.microc.2021.106912.
[34] K. Mervič, V.S. Šelih, M. Šala, J.T. Van Elteren, Non-matrix-matched calibration in bulk multi-element laser ablation – inductively coupled plasma – mass spectrometry analysis of diverse materials, Talanta 271 (2024) 125712, https://doi.org/10.1016/j.talanta.2024.125712.